ParCFD2024
35th International Conference on Parallel Computational Fluid Dynamics
Sep. 02-04, 2024, Bonn, Germany

Data-Driven CFD-Based Design Optimization of Flow Pattern in a Gravitational Mixer Settler

Zinedine Khatir[a,*]

[a] University of Leeds, School of Mechanical Engineering, Woodhouse Lane, Leeds LS2 9JT, UK

ARTICLE INFO[†]

Keywords:
Liquid-Liquid Extraction;
Computational Fluid Dynamics;
Optimization;
Data-Driven Applications

ABSTRACT

Gravitational mixer settlers (GMXSs) are widely used for liquid-liquid extraction (LLE). Immiscible fluids are mixed to promote the transfer of compounds, then separated by gravity in a settling chamber. Micromechanical fluid interactions decisive to the separation process are complex, however studies have shown that by optimizing settler flow pattern, separation performance can be significantly improved. In this paper, an optimization framework for GMXSs designs is investigated which uses experimentally validated single phase Computational Fluid Dynamics (CFD) and residence time distribution (RTD) analyses to identify optimal combinations of design features which maximize desirable characteristics such as resident time and pressure drop. The design of the settler is formulated in terms of two design variables: flow rate and position of the inlet baffle. A Radial Basis Function (RBF)-based surrogate modeling approach using a Design of Experiment (DOE) technique and a permutation genetic algorithm was used to establish optimal process parameters. A Pareto front is built which enables designers to explore appropriate compromises between designs with small residence time and those with small pressure drop.

1. Introduction

Gravitational mixer settlers are used in nuclear [1], chemical, pharmaceutical, and hydrometallurgical industries for liquid-liquid extraction [2, 3]. Processes that define their operation, particularly through the settling chamber, are not fully understood and large equipment means pilot studies are time consuming and costly. CFD provides an alternative method of investigating settler's performance, where gravitational settler analysis has focused on inlet geometric and picket fence configuration by means of multiphase flow analysis [4, 5, 6]. Alternatively, success has been found using single phase simulation to improve settler performance through the flow pattern, and without modeling multiphase coalescence mechanisms [7, 8]. Coalescence is important for settler separation and can be encouraged by minimizing viscous shearing; droplets in the dispersed phase remain in contact for a maximum amount of time, encouraging film drainage and coalescence [9, 10]. Furthermore, for a given system, there exists an optimum residence time over which the separation will satisfactorily occur. It is thus desirable that a maximum proportion of the dispersion flow is in the settler for this time. Lane et al. [8] indicate that plug flow is the ideal regime, but this is practically difficult to achieve, and flow patterns significantly deviate from this ideal, ensuing reduced efficiency. It has been shown in [8, 11] that residence time distribution analysis is adequate to assess settler flow pattern quality.

In the present work, a data-driven CFD-based design-optimization framework is developed with combines surrogate modeling as in [12] and residence time analysis to investigate flow patterns in a GMXS.

2. Materials and method

Figure 1a and Fig. 1b show the geometry of the settler model as depicted by Panda et al. [5].

2.1. Single-phase simulations

The incompressible Navier-Stokes equations for single phase are assumed:

$$\frac{\partial(\rho u)}{\partial t} + \nabla \cdot (\rho u u) - \mu \nabla^2 u = \nabla p, \tag{1}$$

where u denotes fluid velocity, ρ the density, μ viscosity respectively and p its pressure are solved using the `simpleFoam` solver in OpenFOAM subject to the boundary conditions shown in Fig. 1a. These are solved using second order interpolation, an orthogonal hexahedral mesh and under-relaxation factors for velocity and pressure of 0.3 and 0.7 respectively as these are found to provide the best convergence performance. In total, 0.15M elements, as exemplified in Fig. 1b, are used together with automatic parallelization with 8 subdomains minimizing the number of processor boundaries.

[†] This paper is part of the ParCFD 2024 Proceedings. A recording of the presentation is available on YouTube. The DOI of this document is 10.34734/FZJ-2025-02495 and of the Proceedings 10.34734/FZJ-2025-02175.

*Corresponding author
Z.Khatir@leeds.ac.uk (Z. Khatir)
ORCID(s): 0000-0002-7559-7644 (Z. Khatir)

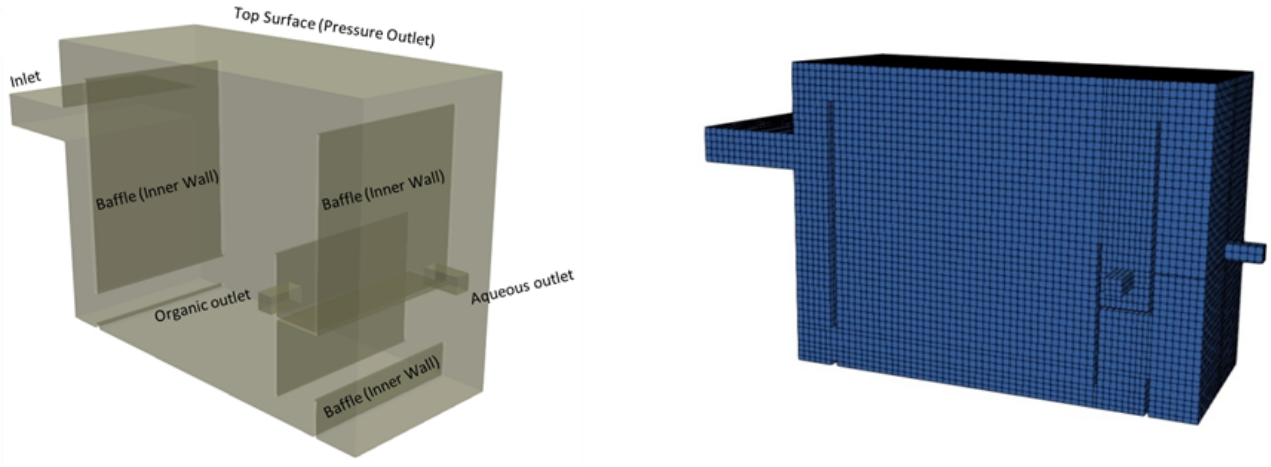

(a) (b)

Figure 1: Schematic of the mixer settler together with: (a) Boundary conditions and (b) example of mesh distribution.

2.2. Residence Time Distribution (RTD)

The cumulative RTD, *F(t)*, is the proportion of the flow with a residence time, *E(t)*, less than or equal to time, *t*. This is calculated by introducing passive scalars at the inlet and calculating the time taken for them to leave the GMXS at the aqueous outlet. The `scalarTransportFoam` solver then solves the convection-diffusion equation for the passive scalar, c, namely

$$\frac{\partial(\rho c)}{\partial t} + \nabla \cdot (uc) - \nabla^2(D_T c) = 0, \tag{2}$$

where the steady, single-phase flow field u is obtained at steady state solution of Eq. (2).

Once *F(t)* is determined, the residence time distribution $E(t)$, the mean residence time t_m, and the standard deviation σ_t are given via

$$E(t) = \frac{d(F(t)}{dt}, \tag{3}$$

$$t_m = \int_0^\infty tE(t)dt, \tag{4}$$

$$\sigma_t = \sqrt{\int_0^\infty (t - t_m)^2 E(t)dt} \quad . \tag{5}$$

The quantity σ_t is useful since a smaller value indicates that the flow is closer to the ideal flow scenario.

2.3. CFD-based optimization strategy

In this section, we consider the optimization of the GMXS system, subject to the conflicting objectives of minimizing both the energy loss, i.e., $E^* = \Delta p \cdot Q \cdot \rho$ with pressure drop Δp, density ρ and flow rate Q, and the RTD σ_t. Two design variables are used, namely: the flow rate Q, and baffle position d_b in the ranges of $0.2\text{m}^3/\text{h} \leq Q \leq 0.8\text{m}^3/\text{h}$ and $55\text{mm} \leq d_b \leq 200\text{mm}$ as indicated in Fig. 2a.

The goal is to generate a Pareto front of non-dominated solutions, from which an appropriate compromise design can be reached. The Pareto front is obtained by building accurate metamodels of both E^* and σ_t, as a function of the two design variables. The metamodels are constructed using values of the E^* and σ_t from numerical simulations carried out at twenty-four Design of Experiments (DOE) points. These points are obtained using Optimal Latin Hypercubes (OLH), by means of a permutation genetic algorithm using the Audze-Eglais potential energy criterion to ensure an efficient distribution of DOE points. The points are laid out as uniformly as possible using criteria of minimizing potential energy of repulsive forces which are inverse square functions of the separation of DOE points [12], i.e.,

$$\min E^{AE} = \min \sum_{i=1}^{N} \frac{1}{L_{ij}^2}, \tag{6}$$

where L_{ij} is the Euclidean distance between points i and j ($i \neq j$) and, $N = 24$ is the number of DOE points. Figure 2b reveals the uniform distribution of the DOE points within the design space as a combination of the design variables Q and d_b.

A Radial Basis Function (RBF) method is used to build the metamodels for E^* and σ_t, throughout the design space where a cubic radial power function is used to determine the weighting (wg) of points in the regression analysis at each point [12], $wg_i = r_i^3$. The parameter r_i is the normalized distance between the surrogate model prediction location from

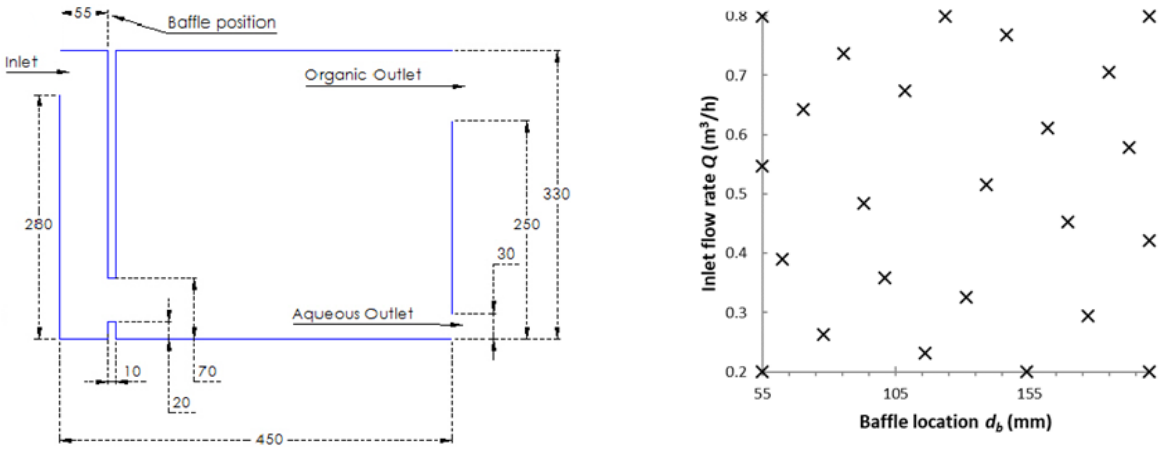

(a) (b)

Figure 2: (a) Two-dimensional plane view indicating the two design variables: Inlet flow rate and baffle position. (b) DOE points distribution.

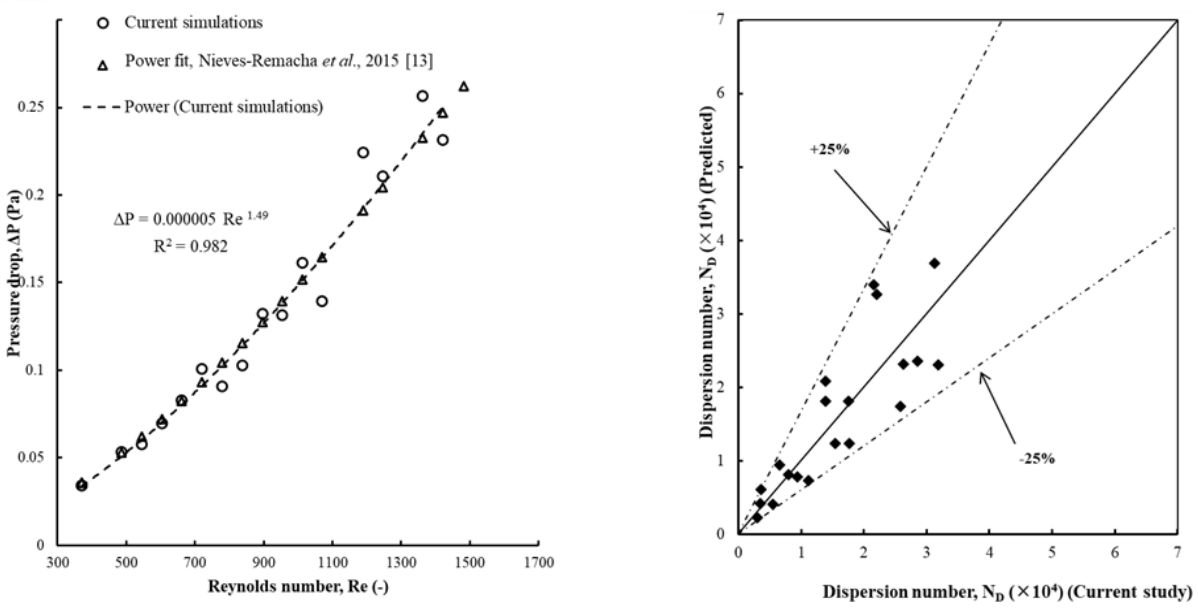

(a) (b)

Figure 3: (a) Pressure drop in the GMXS at different REYNOLDS numbers. The nonlinear behavior is due to the presence of obstacles in the system. (b) Parity plot of the dispersion number N_D.

the i^{th} sampling point. The Pareto front is calculated using a multi-objective genetic algorithm (MOGA) approach as in [12]. Points on the Pareto front are non-dominated in the sense that it is not possible to decrease any of the objective functions (i.e., E^* and σ_t) without increasing the other objective function. Hence, this provides designers the opportunity to select the most convenient compromise point among the optimum designs. In the next section, results of the data-driven CFD-based design optimization are discussed.

3. Results and discussion

3.1. Validation of the method

Simulations are performed with corresponding RTD flow analysis. Results are firstly validated against the work by Nieves-Remacha [13], Fig. 3a, with the pressure drop found to follow a similar power law $\Delta P \approx Re^{1.49}$ where the nonlinear effect is due to the presence of baffles in the settler and Re is the REYNOLDS number.

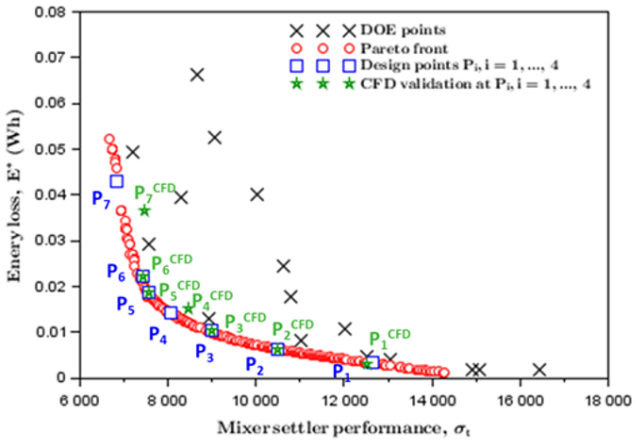

Figure 4: Pareto front showing the compromises that can be obtained in minimizing both σ_t and E^*.

The effectiveness of separation is expressed in terms of following dimensionless number dispersion number (N_D) as noted by Manavalan et al. [14] such as

$$N_D = \frac{1}{t_m}\sqrt{\frac{H}{g}}, \tag{7}$$

where t_m is the mean residence time as defined in the RTD analysis, g the acceleration due to gravity and H is the dispersion-band thickness using the correlation developed by Panda & Buwa [6]. A parity plot of the dispersion number N_D between the prediction by Jeelani and Hartland [15] and the current work is presented in Fig. 3b.

4. Optimization

The Pareto front curve in Fig. 4 represents the results in terms of both σ_t and E^*. The data reveal that any decrease of E^* or σ_t is followed by an increase of the other objective function. A very good agreement between the metamodel and full numerical calculations occurs demonstrating the accuracy of the metamodeling approach implemented. Results reveal that at point P_4, identified to be the best compromise design, a percentage error for around 5% and 6% for energy E^* and σ_t between the CFD predictions and metamodels suggesting the appropriateness of the data-driven model to predict accurately E^* and σ_t. Further analysis, as depicted in Fig. 5a, indicates point P_4 to provide $E^* = 0.0142$mWh and $\sigma_t = 8062$. The Pareto and E-curves in Fig. 5b might indicate point P3 to be also a good design, however this corresponds to an increase of 11.4% and 25.4% in E^* and σ_t respectively, compared to P_4. Though the E-curves, Fig. 5b, recommend point P_7 to be a good design, an increase of 203% in E^* is observed compared to P_4 then again.

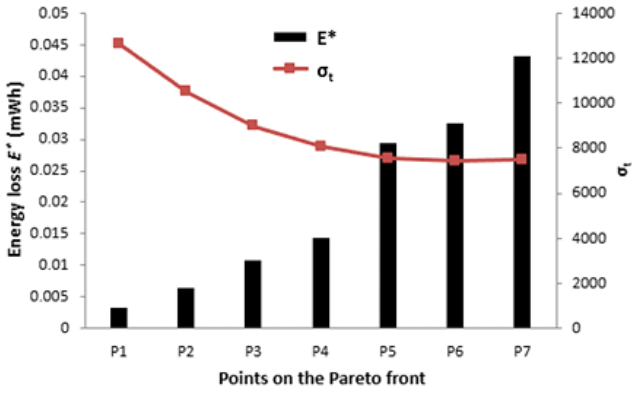

(a)

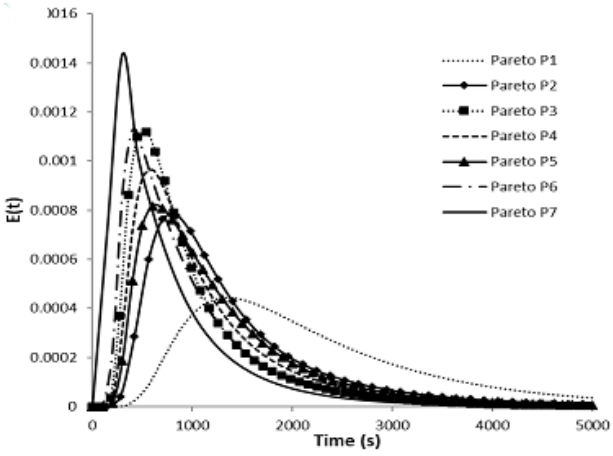

(b)

Figure 5: (a) Energy loss E^* and σ_t and, and (b) RTD $E(t)$ at seven points on the Pareto front in Fig. 4.

Design P_4 corresponds to a flow rate $Q = 472\text{m}^3/s$ and a baffle position $d_b = 139$mm.

5. Conclusions

A data-driven CFD-based optimization methodology has been successfully developed for the design of efficient GMXS liquid-liquid extraction systems. Current work entails a multi-fidelity approach which combines multiphase flow analysis.

Data statement

All data underlying the results are available as part of the article and no additional source data are required in the Research Data Leeds Repository[1].

[1] https://doi.org/10.5518/1578

References

[1] D. B. Sharma, S. A. Ansari, R. B. Gujar, P. K. Mohapatra, Demonstration of Mixer-Settlers Runs for Separation of Uranium and Neptunium by TBP Vis-a-Vis DHOA Under a Legacy Waste Condition, Solvent Extraction and Ion Exchange 42 (3) (2024) 264–280. doi:10.1080/07366299.2024.2360504.

[2] D. Hadjiev, J. Paulo, Extraction separation in mixer–settlers based on phase inversion, Separation and Purification Technology 43 (3) (2005) 257–262. doi:10.1016/j.seppur.2004.11.006.

[3] J. M. Martins, A. S. Guimarães, A. J. B. Dutra, M. B. Mansur, Hydrometallurgical separation of zinc and copper from waste brass ashes using solvent extraction with D2EHPA, Journal of Materials Research and Technology 9 (2) (2020) 2319–2330. doi:10.1016/j.jmrt.2019.12.063.

[4] S. Ye, Q. Tang, Y. Wang, W. Fei, Structural optimization of a settler via CFD simulation in a mixer-settler, Chinese Journal of Chemical Engineering 28 (4) (2020) 995–1015. doi:10.1016/j.cjche.2020.01.010.

[5] S. K. Panda, K. Singh, K. Shenoy, V. V. Buwa, Numerical simulations of liquid-liquid flow in a continuous gravity settler using OpenFOAM and experimental verification, Chemical Engineering Journal 310 (2017) 120–133. doi:10.1016/j.cej.2016.10.102.

[6] S. K. Panda, V. V. Buwa, Effects of Geometry and Internals of a Continuous Gravity Settler on Liquid–Liquid Separation, Industrial & Engineering Chemistry Research 56 (46) (2017) 13929–13944. doi:10.1021/acs.iecr.7b03756.

[7] D. Stanbridge, J. Sullivan, One example of how offshore oil & gas industry technology can be of benefit to hydrometallurgy., in: Second International Conference on CFD in Minerals and Process Industries CSIRO, Melbourne, Australia, 1999, pp. 317–321.
URL https://www.cfd.com.au/cfd_conf99/Conf99_Papers/067STAN.PDF

[8] G. L. Lane, K. Mohanarangam, W. Yang, D. J. Robinson, K. R. Barnard, Flow pattern assessment and design optimisation for an industrial solvent extraction settler through in situ measurements and CFD modelling, Chemical Engineering Research and Design 109 (2016) 200–214. doi:10.1016/j.cherd.2016.01.021.

[9] J. Kamp, J. Villwock, M. Kraume, Drop coalescence in technical liquid/liquid applications: a review on experimental techniques and modeling approaches, Reviews in Chemical Engineering 33 (1) (2017) 1–47. doi:10.1515/revce-2015-0071.

[10] S.-l. Yan, X.-q. Wang, L.-t. Zhu, X.-b. Zhang, Z.-h. Luo, Mechanisms and modeling of bubble dynamic behaviors and mass transfer under gravity: A review, Chemical Engineering Science 277 (2023) 118854. doi:10.1016/j.ces.2023.118854.

[11] G. Miller, Design of mixer-settlers to maximise performance, in: Design of mixer-settlers to maximise performance, ALTA Metallurgical Services, Melbourne, Australia, 2006.

[12] M. Al-Damook, Z. Khatir, M. Al Qubeissi, D. Dixon-Hardy, P. J. Heggs, Energy efficient double-pass photovoltaic/thermal air systems using a computational fluid dynamics multi-objective optimisation framework, Applied Thermal Engineering 194 (2021) 117010. doi:10.1016/j.applthermaleng.2021.117010.

[13] M. J. Nieves-Remacha, A. A. Kulkarni, K. F. Jensen, OpenFOAM Computational Fluid Dynamic Simulations of Single-Phase Flows in an Advanced-Flow Reactor, Industrial & Engineering Chemistry Research 54 (30) (2015) 7543–7553. doi:10.1021/acs.iecr.5b00232.

[14] B. Manavalan, T. V. Tamhane, J. Patra, A. J. Joshi, J. B. Joshi, N. K. Pandey, S. Kumar, K. U. Mudali, N. Rajamani, V. S. Vitankar, R. N. Patil, Separation Characteristics of Liquid– Liquid Dispersions: Gravity and Centrifugal Settlers, Industrial & Engineering Chemistry Research 56 (27) (2017) 7814–7823. doi:10.1021/acs.iecr.7b00119.

[15] S. A. K. Jeelani, S. Hartland, Prediction of steady state dispersion height from batch settling data, AIChE Journal 31 (5) (1985) 711–720. doi:10.1002/aic.690310503.